BIOCHEMISTRY
including biophysical chemistry & molecular biology

Article

pubs.acs.org/biochemistry

Activation of a Unique Flavin-Dependent tRNA-Methylating Agent

Djemel Hamdane,*[,†] Eduardo Bruch,[‡] Sun Un,[‡] Martin Field,[§] and Marc Fontecave[†]

[†]Laboratoire de Chimie des Processus Biologiques, CNRS-FRE 3488, Collège De France, 11 place Marcelin Berthelot, 75231 Paris Cedex 05, France

[‡]Service de Bioénergétique, Biologie Structurale et Mécanismes (CNRS UMR-8221), Institut de Biologie et de Technologies de Saclay, CEA-Saclay, F-91191 Gif-sur-Yvette, France

[§]DYNAMO/DYNAMOP, Institut de Biologie Structurale − Jean-Pierre Ebel, UMR 5075 − CEA/CNRS/UJF, 41 rue Jules Horowitz, 38027 Grenoble Cedex 1, France

Supporting Information

ABSTRACT: TrmFO is a tRNA methyltransferase that uses methylenetetrahydrofolate (CH_2THF) and flavin adenine dinucleotide hydroquinone as cofactors. We have recently shown that TrmFO from *Bacillus subtilis* stabilizes a TrmFO−CH_2−FADH adduct and an ill-defined neutral flavin radical. The adduct contains a unique N−CH_2−S moiety, with a methylene group bridging N^5 of the isoalloxazine ring and the sulfur of an active-site cysteine (Cys53). In the absence of tRNA substrate, this species is remarkably stable but becomes catalytically competent for tRNA methylation following tRNA addition using the methylene group as the source of methyl. Here, we demonstrate that this dormant methylating agent can be activated at low pH, and we propose that this process is triggered upon tRNA addition. The reaction proceeds via protonation of Cys53, cleavage of the C−S bond, and generation of a highly reactive $[FADH(N^5){=}CH_2]^+$ iminium intermediate, which is proposed to be the actual tRNA-methylating agent. This mechanism is fully supported by DFT calculations. The radical present in TrmFO is characterized here by optical and EPR/ENDOR spectroscopy approaches together with DFT calculations and is shown to be the one-electron oxidized product of the TrmFO−CH_2−FADH adduct. It is also relatively stable, and its decomposition is facilitated by high pH. These results provide new insights into the structure and reactivity of the unique flavin-dependent methylating agent used by this class of enzymes.

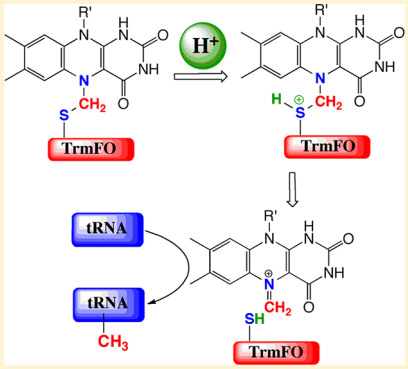

Folate- and FAD-dependent methyltransferase (TrmFO) is a ∼50 kDa flavoenzyme that is expressed in Gram-positive bacteria. It is involved in the methylation of uridine at position 54 in tRNAs, which forms the widely conserved 5-methyluridine54 (m^5U_{54}).[1,2] m^5U_{54} together with adenine 58 makes up a reverse Hoogsteen base pair that contributes to the stabilization of the L-shaped structure of the tRNA.[3] As shown by labeling experiments, the N^5,N^{10}-methylenetetrahydrofolate cofactor (CH_2THF) constitutes the source of carbon in the form of a methylene group, whereas the electrons required for the reduction of this methylene into a methyl moiety are provided by a flavin adenine dinucleotide hydroquinone ($FADH_2$).[2,4−6] Although this metabolic pathway was discovered more than 30 years ago by Delk et al., a relevant enzymatic mechanism was proposed only recently on the basis of our investigations of TrmFO from *Bacillus subtilis*.[7−9] In an earlier study, we reported that an active tRNA-methylating species was present in freshly purified preparations of recombinant TrmFO.[7] By a combination of spectroscopic, biochemical, and mass spectrometry analyses,[9] the chemical nature of this species was later unambiguously identified as a unique flavin−protein adduct in which a methylene covalently bridges nitrogen N^5 of reduced FAD to the sulfur atom of an essential cysteine (Cys_{53}) (Figure 1). This species was proposed to derive from methylene transfer from CH_2THF to N^5 of $FADH_2$ followed by nucleophilic addition of cysteinate 53.[9]

Obviously, this novel methylating agent contains all of the ingredients required to methylate the tRNA substrate (i.e., a methylene group and a hydride equivalent carried by the flavin). In the absence of tRNA, this species is remarkably stable

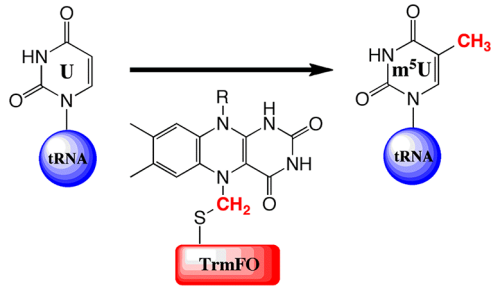

Figure 1. tRNA methylation catalyzed by TrmFO. The chemical structure of the catalytically competent TrmFO−CH_2−FAD methylating adduct is shown.

Received: October 10, 2013
Revised: November 14, 2013
Published: November 14, 2013

in neutral pH aqueous solutions. In contrast, addition of tRNA transcripts readily activates it, allowing spontaneous uridine methylation. When a mini-RNA containing 5-fluorouridine was used as a substrate instead, the reaction generated a stable covalent RNA−protein adduct resulting from nucleophilic addition of Sγ-Cys226 onto the C6 atom of the targeted uridine.[8] The presence of a fluorine atom at C5 prevented further development of the reaction. This result established Cys226 as a critical residue for substrate activation through a mechanism shared by most DNA and RNA C5-modifying methyltransferases.[10−13] All of these data have been recently translated into a novel mechanism for flavin-dependent methylation of C5−U_{54} by TrmFO.[9] These results provided a new and exciting facet of the versatile reactivity of flavins.

The stability of the FAD−protein-methylating species (henceforth referred to as MS) in the absence of tRNA substrate is intriguing. To obtain some insight into the activating mechanisms, we have studied the behavior of MS in the absence of tRNA under various pH and denaturing conditions, and we show that activation can be simply achieved by protonation. From this, we propose a general acid-catalysis mechanism, fully supported by DFT calculations, for the activation of the TrmFO dormant tRNA-methylating species. We have extended this study to the one-electron oxidized derivative, an original, still ill-defined, stable radical species that is also present in fresh TrmFO preparations but is catalytically inactive. By combining optical, high-field EPR/ENDOR spectroscopy, and DFT calculations, we have characterized it completely for the first time. This radical, remarkably stable at neutral and acid pH, in contrast with its reduced precursor, can be decomposed only at high pH.

METHODS

Protein Preparations. Recombinant N-terminus $(His)_6$-tagged TrmFO from *Bacillus subtilis* was expressed and purified as reported.[14] The proteins purity was >95%, as judged by SDS-PAGE. The protein was concentrated to ≈500−800 μM in 50 mM Tris-HCl, pH 7.8, 150 mM NaCl, and 10% (v/v) glycerol and stored at −80 °C. Pure photolyase from *Aspergillus nidulans* was a gift from Klaus Brettel (CEA Saclay, France) and André Eker (Erasmuus University Medical Center, Rotterdam, The Netherlands)

UV−Vis Spectroscopy. All UV−vis absorption spectra were recorded from 250 to 750 nm on a Cary 50 spectrophotometer (Varian) at room temperature. The pH dependence of the absorption spectrum of TrmFO was studied from pH 6 to 11 (50 mM potassium phosphate from 6 to 8, 50 mM Tris-HCl + 150 mM NaCl for pH 8, and 50 mM CAPS for pH 10 to 11). Decay kinetics of the alkylated flavin adducts were followed spectrophotometrically after mixing 10−30 μM TrmFO containing the FAD adducts with oxygenated buffer at various pH values in a 1 cm path length quartz cuvette.

Fluorescence Spectroscopy. Fluorescence spectra of TrmFO (2 to 5 μM) were recorded on a Cary Eclipse fluorescence spectrophotometer (Varian) with excitation and emission slit widths of 5 nm. When the flavin was excited at 450 nm, emission was monitored from 465 to 700 nm. Upon excitation of TrmFO tryptophans at 295 nm, emission was monitored from 310 to 500 nm.

EPR and ENDOR Spectroscopy. The HFEPR spectrometer has been described in detail elsewhere.[7,15] Field calibration was based on a small Mn(II)-doped MgO standard sample (g = 2.000101) mounted immediately above the frozen sample. The 95 GHz ENDOR and PELDOR spectra were obtained at 40 to 90 K using a Bruker Elexsys II 680 EPR spectrometer equipped with a Bruker power upgrade 2, Amplifier Research 500 W radiofrequency amplifier, and an Oxford Instruments CF935 flow cryostat. The Davies ENDOR were obtained using an initial 200 ns microwave inversion pulse followed by a 20 μs radio frequency excitation of the nuclear spins, and the detection was achieved using an echo detection composed of 10 and 20 ns pulses. The calculated g-values and hyperfine couplings of the neutral FAD radical (N_5−H) and its N_5-substituted derivates with N_5−CH_3, N_5−CH_2−OCH_3, and N_5−CH_2−SCH_3 were obtained using the Gaussian 09 (revision C.01) package. Isoalloxazine with an (N_{10})−CH_2−CH_2OH−CH_3 group served as a model for the FAD molecules (Figure S1). The structures were geometry optimized using the B3LYP/6-31+G(D,P) functional and basis-set combination. The g-values were calculated using the same combination, whereas the hyperfine couplings were calculated using the PBE0PBE/EPR-III combination (except for the sulfur atom, for which the 6-31+G(D,P) basis set was used). For more details regarding the approaches taken, see ref 16. The effect of the angular position of the SCH_3 group on the spin parameters was calculated by rotating the N_5−CH_2(SCH_3) bond of the optimized structure without further geometry optimization. The sulfur position was defined by the S−C−N_5−$C_{4\alpha}$ dihedral angle (Figure S1). In the following, A_{iso} refers to the isotropic part and T_{ii} (*ii* = *xx*, *yy*, and *zz*) refers to the principal values of the anisotropic component of the hyperfine interactions.

pH-Dependent Reactions: DFT Calculations. For quantum chemical calculations, a density functional theory (DFT) approach was used on model systems representing the reduced and radical forms of FAD and adjacent residue Cys53. All calculations were done with a triple-ζ TZVP basis set[17] and the COSMO implicit solvent model.[18] To check the dependence of the results of the DFT approach, all calculations were duplicated with two functionals, B3LYP[19] and BP86,[20] as representatives of the hybrid and GGA classes of functional, respectively. Likewise, all calculations were done in two models of solvent, hexane and water, to mimic the two extremes of environment, protein and bulk water, to which the model FAD system could possibly be exposed. The ORCA program package was employed for all electronic structure calculations.[21]

The model system that was chosen was the isoalloxazine portion of the FAD, terminated at the N^{10} atom by a methyl group. The Cys53−CH_2− attachment to the flavin was represented by a CH_3−S−CH_2− group attached to the N^5 atom of the flavin (Figure S4B). Reduced and radical forms of this model were constructed, and the geometry was optimized in implicit solvent. Starting from this basic model, two types of calculation were performed, namely, the determination of the energies of possible reactions involving the FAD−CH_2−Cys53 adduct and the generation of hypothetical energy profiles for acid and base attack. For the reaction energies, all species, including derivatives of the adduct, were geometry optimized in the appropriate implicit solvent. For the energy profiles, we employed $H3O^+$ and OH^- to represent acid and base, respectively, and we used a scanning approach in which successive geometry optimizations were performed at different fixed distances between the target atom and either the hydronium proton or hydroxide oxygen.

dx.doi.org/10.1021/bi4013879 | *Biochemistry* 2013, 52, 8949−8956

Table 1. Measured g- and Hyperfine Values of TrmFO and *A. nidulans* Photolyase Neutral FAD Radicals and Calculated B3LYP/6-31+ G(D,P) g-Values and PBE0PBE/EPR-III Hyperfine Coupling Constants of the Corresponding FAD-S-$CH_3^{\bullet}$, FAD-O−$CH_3^{\bullet}$, and $FADH^{\bullet}$ Radical Models[a]

	g_x	g_y	g_z	g_{iso}	A_{iso}	T_{xx}	T_{yy}	T_{zz}
TrmFO								
pH 8	2.00504	2.00441	2.00258	2.00388	20[b] (N−C**H**−S)	N.D.	N.D.	N.D.
pH 11	2.00465	2.00448	2.00251	2.00401	20[b] (N−C**H**−S)	N.D.	N.D.	N.D.
photolyase	2.00440	2.00370	2.00220	2.00344	30[b] (N−**H**)	N.D.	N.D.	N.D.
B3LYP/6-31+ G(D,P)					PBE0PBE/EPR-III			
In Vacuo								
N−H	2.00453	2.00399	2.00204	2.00352	−23.7 (N−H)	−16.7	−4.0	20.9
N−CH_3	2.00467	2.00406	2.00213	2.00362				
N−CH_2−OMe (79° O)	2.00466	2.00395	2.00213	2.00358				
N−CH_2−SMe (77° S)	2.00557	2.00437	2.00245	2.00413	13.6 (N−CH−S)	−2.9	−2.0	4.9
N−CH_2−SMe[c] (60° S)	2.00502	2.00439	2.00237	2.00393	26.7 (N−CH−S)	−2.8	−2.2	5.0
N−CH_2−SMe[c] (38° S)	2.00472	2.00443	2.00242	2.00386	43.6 (N−CH−S)	−2.8	−2.2	5.0
ε = 20								
N−**H**	2.00439	2.00373	2.00202	2.00338	−26.0	−18.5	−4.2	22.7
N−CH_2−**SMe** (89° S)	2.00539	2.00414	2.00244	2.00399	12.9	−3.0	−2.0	5.0
N−CH_2−SMe[c] (60° S)	2.00521	2.00400	2.00240	2.00387	34.3	−3.4	−0.3	3.8
N−CH_2−SMe[c] (118° S)	2.00767	2.00404	2.00066	2.00413	57.8	−2.7	−1.1	3.9

[a]*A* and *T* values are given in MHz. [b]The sign is assumed from calculations. [c]Calculated using the optimized geometry with a modified dihedral angle. The optimal dihedral angles were 77° (in vacuo) and 89° (ε = 20).

RESULTS AND DISCUSSION

Characterization of the Radical Present in TrmFO by High-Field EPR/ENDOR and DFT Calculations. Freshly purified preparations of TrmFO contain an air-stable catalytically inactive FAD-derived organic radical that can be monitored by UV−vis and EPR spectroscopy.[7] Our original analyses of the high-field EPR and ENDOR spectroscopy of the TrmFO radical left two features unexplained. The first was its unusual g-values, which were higher than those previously reported for similar radicals. In particular, its g_z tensor component, which is directed along the ring-perpendicular component, was considerably higher than the free-electron g-value of 2.00232 (Table 1). It has been shown theoretically that the ring-perpendicular component of the g-tensor of planar organic π radicals should lie below the free-electron value because of relativistic effects. This is the case for semiquinones, tyrosyl radicals, and flavosemiquinones.[22−26] The proton ENDOR resonances at ±10 MHz were another unusual feature of the TrmFO radical. These were originally assigned to one of the ribityl C_1−H protons.[7] The hyperfine interaction of such a peripheral proton strongly depends on its position with respect to the π-bonding network.[27] The relatively large 20 MHz hyperfine coupling was proposed to have arisen from one of the C_1−H protons positioned perpendicular to the ring in a manner that is significantly different from all of the other flavosemiquinones that have been studied.

With the knowledge that the radical was cross-linked to the sulfur side chain of a cysteine from the protein,[9] we re-examined the EPR spectra of the TrmFO FAD radical. In particular, a detailed comparison of its EPR and ENDOR spectra was made with those of the neutral *Aspergillus nidulans* photolyase standard FAD radical, and a series of DFT calculations were carried out to determine its theoretical g- and hyperfine tensors. The $FADH^{\bullet}$ radical in photolyase was used as a reference to base our interpretation of the high-field EPR/ENDOR spectroscopic properties of the TRMFO radical because the structure of this protonated radical and its environment were known from crystallography and its EPR and ENDOR spectra were well-characterized.[27,25]

The 285 GHz EPR spectra of TrmFO and photolyase radicals were significantly different (Figure 2). The principal g-

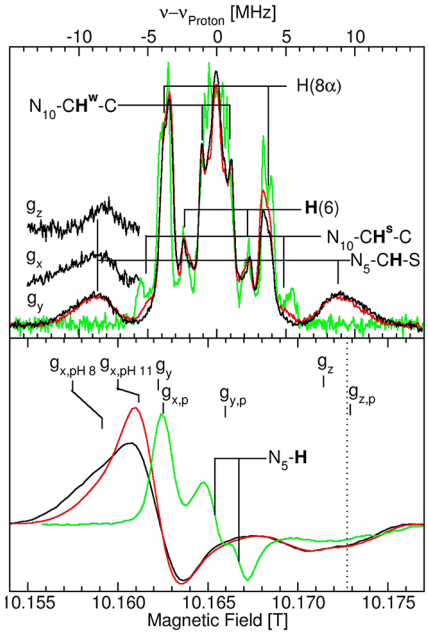

Figure 2. High-field EPR and ENDOR spectra. The 285 GHz EPR (bottom) and 95 GHz Davies pulse ENDOR (top) spectra of TrmFO (black, pH 8; red, pH 11) and *A. nidulans* photolyase FAD radicals (green). g_i and $g_{i,p}$ (i = *x*, *y*, and *z*) are principle g-values of the TrmFO and photolyase radical, respectively. $g_{x,pH8}$ and $g_{x,pH11}$ are g_x values of the TrmFO radical at pH 8 and 11, respectively. The dotted line marks the magnetic field corresponding to the free-electron g-value. The complete ENDOR spectra were recorded at the magnetic field corresponding to the g_y values of the respective radicals. Portions of the pH 8 TrmFO radical ENDOR taken at the g_x and g_z field positions are also shown. The larger couplings are labeled.

dx.doi.org/10.1021/bi4013879 | *Biochemistry* 2013, 52, 8949−8956

values of the photolyase radical were consistent with those measured for other photolyase FAD radicals[27,25] and were lower than the corresponding values for the TrmFO radical (Table 1). Its g_z value fell below the free-electron g-value. There was no evidence of the large photolyase N^5−**H** hyperfine coupling (13 G or 36 MHz) in the TrmFO spectra (Figure 2). Hyperfine couplings give direct information about the ground-state spin distribution of the unpaired electron of a radical and hence about its electronic structure. The smaller couplings that could not be directly measured from the EPR spectra were obtained using ENDOR. In contrast to their high-frequency EPR spectra, the ENDOR spectra of these two radicals were essentially identical (Figure 2). The ENDOR resonances could be readily assigned on the basis of previous work on other flavin radicals.[25,26] The larger couplings are labeled in Figure 2. Photolyase and TrmFO radicals had the same **H**(8α), **H**(6), and N^{10}−C**H**$_2$−C couplings, indicating that the delocalization of the unpaired electron was very similar in the two molecules. (However, the amplitudes of these ENDOR resonances differed, reflecting difference in the g-tensors of the radicals.) The sizes of the two N^{10}−C**H**$_2$ proton hyperfine coupling constants (indicated as N^{10}−C$\mathbf{H}^S$ and N^{10}−C$\mathbf{H}^W$ in Figure 2) depend on their angular orientations with respect to the flavin ring, reaching a maximum value when the C−H bond is perpendicular to the ring plane and parallel with the N^{10} p_z orbital. Such proton hyperfine interactions are also largely isotropic and do not change when they are measured at different magnetic-field values. The nearly identical values for the photolyase and TrmFO radicals indicate that the orientations of the N^{10}−C**H**$_2$ protons are essentially identical in both radicals. As discussed above, we initially proposed that this was not the case and that the unique ±10 MHz ENDOR resonances present in the spectrum of the TrmFO radical reflected different orientations of these protons. With this not being the case, not only must the TrmFO radical have extra protons not present in the photolyase radical but also these protons experience a large 20 MHz hyperfine coupling interaction. This coupling was largely insensitive to orientation because ENDOR taken at the g_x, g_y, and g_z field positions showed that it was nearly isotropic. These observations were consistent with coupling with one of the N^5−C**H**$_2$−S protons.

DFT calculations were carried out to understand quantitatively how the N^5−CH_2−S− cross-link affected the nature of the radical and its magnetic spin parameters (Table 1). The quality of such calculations in predicting the g-values and hyperfine coupling constants can be appreciated by comparing the calculated values with those measured for the photolyase radical. The differences between the experimental and calculated in vacuo g-values are smaller than ±0.0003 and are even smaller for values calculated for the radical embedded in a medium with a dielectric constant of 20. In the latter case, the only significant discrepancy is the underestimated g_z value. The 30 MHz N^5−H hyperfine coupling in the photolyase radical is also reproduced by the calculations. The effect of the cross-linking group was examined using a flavosemiquinone model having a N^5−CH_2−S−CH_3 group (Figure S1). The DFT calculations reproduced all of the salient features of the experimental data. The presence of the cross-link shifted the g-values upward relative to those of the simple flavin radical, bringing the g_z component well above the free-electron value, although not as much as the measured value. The marked increase in g-values because of the cross-link was specifically a result of the sulfur atom. The effect of a N−CH_2−O−CH_3 group was indistinguishable from that of a N−CH_3 or N−H group (Table 1). The hyperconjugation interaction between the bigger sulfur atom and the N^5 p_z orbital is likely to be larger than those of hydrogen or oxygen atoms. In addition, the heavier sulfur atom will make larger contributions to both the spin−orbital and relativistic components of the g-tensor. The latter is presumably responsible for the deviation of the g_z component to larger than free-electron values. In the optimized geometry of the model radical, the C−S bond was 23° relative to the ring-perpendicular. Improved agreement between the experimental and calculated g-values could be obtained when this angle was increased to 30° as well as when embedding the radical in a dielectric medium (Table 1).

As the calculations show, the changes in the angular positions of the −CH_2−S atoms with respect to the flavin ring plane will not only strongly modulate the g-values but also the proton hyperfine couplings (Table 1). Although the g-values of the TrmFO radical are pH dependent, its hyperfine couplings are not. This means that it is unlikely that a simple rotation about the N^5−CH_2S bond is responsible for the pH dependence because the angular positions of the proton and sulfur atoms change in a concerted manner. Calculations using different dielectric media suggest that one possible explanation is that the interaction between the sulfur atom and the flavin π-bonding network is affected by changes in the local electrostatic environment, such as a nearby ionization event unassociated with the radical itself. The high-field EPR and ENDOR measurements and DFT calculations show that the magnetic spin parameters of the TrmFO radical are consistent with the N−CH_2−S− cross-link but that this cross-link does not affect the ground-state electronic structure of the FAD radical.

Stability of TrmFO−FAD Adducts: pH Effects. Freshly purified enzyme was directly diluted in buffers at different pH values (6, 7, 8, and 10) under aerobic conditions and in the absence of tRNA. A small volume of concentrated protein at pH 8 was added to a large volume of buffer to avoid any pH modification of the medium. We were not able to investigate lower pH conditions because the protein was prone to precipitate and aggregate at low pH. The initial UV−vis spectrum exhibited a complex shape, reflecting the presence of three FAD species: MS absorbing light exclusively below 400 nm, the radical with a broad band between 515 and 750 nm, and noncovalently bound FAD in its oxidized state absorbing at 445 nm (Figure S2). MS was remarkably stable for several hours at pH 10, whereas its conversion directly to FAD could be observed by lowering the pH, with a relatively fast process at pH 6. In contrast, at pH 6, the bands characteristic of the radical did not change after prolonged incubation, whereas at increased pH, the radical was also slowly converted to FAD. The difference spectra (insets of Figure S2) obtained by subtracting the initial spectrum from the final one are consistent with the reaction proceeding toward the formation of FAD. Evidence that the FAD product did not remain covalently attached to TrmFO was obtained by a treatment of the pH 8 reaction mixture, pH conditions under which both adducts decomposed, with 0.2% SDS at the end of the reaction. The complete release of FAD from the protein after SDS treatment has been confirmed by separation of apo-enzyme and flavin on a gel G-25 filtration. The release of free FAD indicated that the N^5−CH_2 bond was broken during the reaction.

The kinetics of decomposition of MS and the radical under the various pH conditions were obtained by monitoring the absorbance variations at 445 and 600 nm, respectively, as a

dx.doi.org/10.1021/bi4013879 | Biochemistry 2013, 52, 8949−8956

function of time (Figure 3). The decrease of absorption at 600 nm can indeed be exclusively assigned to a loss of the radical.

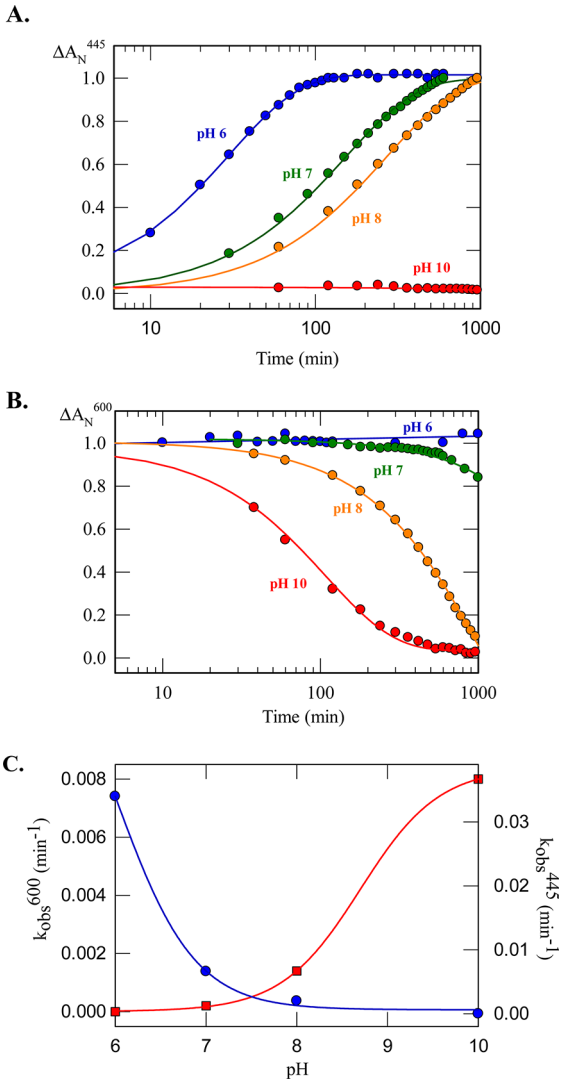

Figure 3. Kinetics of conversion of the TrmFO–FAD adducts to oxidized FAD. (A) MS decomposition, monitored at 445 nm. (B) Radical decomposition, monitored at 660 nm. The normalized kinetics traces at 445 (A) and 600 (B) nm were fitted to monoexponential $\Delta A_N(t) = \exp(-k_{obs}t)$. The pH dependence of the rate constants k_{obs} are shown in panel C.

Variations of the absorbance at 445 nm, monitoring the formation of FAD, can be used to monitor MS concentration variations because light absorption of the radical at 445 nm is not significant and conversion of the radical into FAD results in very little variation at 445 nm because of a large difference in extinction coefficients between the radical and FAD. As shown in Figure 3A,C, the decay of MS was essentially monophasic at all tested pH values. Going from pH 6 to 8, the rate constant of the reaction decreased by a factor of ~17, and the reaction did not proceed at pH 10. In contrast, the observed rate constant for radical decomposition increased by a factor of 20 upon increasing the pH from 7 to 10 (Figure 3B,C). Therefore, in the absence of tRNA, low pH accelerates the decomposition of MS, whereas it slows down that of the radical. Interestingly, the rate constant of the decay of MS at pH 8 in the presence of tRNA is approximately 1 order of magnitude larger than the one determined at pH 6 in the absence of tRNA.[7,8]

Stability of TrmFO–FAD Adducts: Denaturation Effects. To determine whether the decomposition of the adducts in the absence of tRNA is mediated by an amino acid acting as a general acid/base catalyst, the decomposition kinetics were measured under denaturing conditions using urea as a chaotropic agent. Fluorescence studies established that a concentration of urea of 2 M was sufficient to unfold the protein completely and to release the noncovalently bound FAD (Figure S3A,B). Under these conditions, the radical disappeared within a few minutes. In contrast, MS conversion to FAD occurred at a rate comparable to that determined in the absence of urea (0.01 vs 0.007 min^{-1}, respectively) (Figure S4A,B). Therefore, the last reaction is insensitive to denaturation, suggesting that protonation of the adduct in the absence of tRNA is not assisted by an amino acid of the protein but that it more probably depends directly on the solvent.

DFT Analysis of the Reaction of TrmFO–FAD Adducts with Acid and Base. The computational results from the calculations with the B3LYP and BP86 functionals were very similar, so we only employ those obtained with B3LYP here. Similarly, inspection of the available crystal structures of TrmFO from *Thermus thermophilus* (PDB codes 3G5Q, 3G5R, and 3G5S) shows that one side of the flavin ring and the side chain of the adjacent Cys residue is exposed to solvent, implying that the results obtained with an implicit water model are likely to be more pertinent than those in hexane (Figure S5A). In any case, the major differences between the hexane and water results occur in the reaction energies, as water strongly penalizes ion desolvation, especially for the smaller H_3O^+ and OH^- species.

Atomic (ESP) charge, spin, and bond-order analyses were performed on the geometry-optimized model systems (structure of the model shown in Figure S5B). These showed that the radical spin was located mostly on the C$^4\alpha$ and N^5 atoms of the flavin, with a small amount also on N^{10}, and that there was a significant increase in the electrophilicity of the N^5 atom on going from the reduced to radical forms, with a corresponding increase in the nucleophilicity of the atoms to which it was bound (C4α, C5α, and CH_2). The bond orders of the bonds involving CH_2 were very similar for the two forms, with a slight weakening and strengthening of the radical N^5–CH_2 and CH_2–S bonds, respectively.

Acid Attack. Protonation of the S atom of the reduced model system leading to the formation of the flavin methylene iminium [FADH(N^5)=CH_2]$^+$ and liberation of CH_3SH is an energetically favorable reaction (−79 kJ/mol) (Figure S6). Protonation at N^5 and O^4 is also favorable but is not mechanistically relevant. In contrast, for the radical model system, the reaction is highly energetically unfavorable (+48 kJ/mol). These reaction energies, in full agreement with experimental observations, show that decomposition of the model system under acid attack is favored in the reduced but not the radical form. To obtain an estimate of the barriers to decomposition, reaction profiles were generated by approaching the hydronium to the S atom of the N–CH_2–S system. For the reduced form, this is a barrierless and exothermic process ($\Delta E \sim -80$ kJ/mol) that results in the rupture of the C–S bond, yielding the flavin [FADH(N^5)=CH_2]$^+$ iminium with liberation of CH_3–SH and H_2O (Figure S6). The energy profile for protonation of S in the radical is also barrierless and slightly exothermic ($\Delta E \sim -20$ kJ/mol), but even at S–H

dx.doi.org/10.1021/bi4013879 | *Biochemistry* 2013, 52, 8949–8956

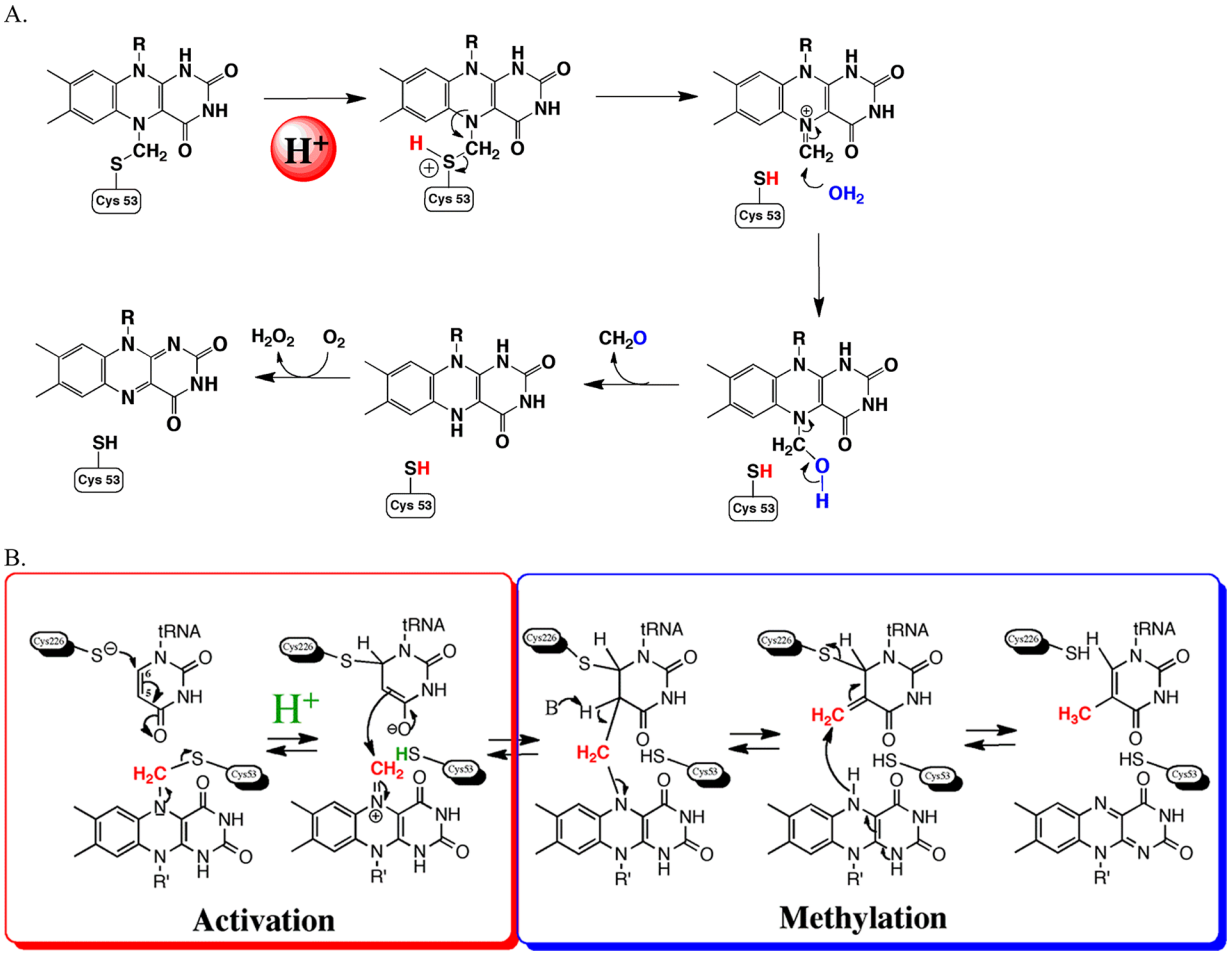

Figure 4. Proposed mechanisms for activation of the TrmFO−FAD-methylating adduct. (A) In the absence of tRNA, decomposition. (B) In the presence of tRNA, methylation of uridine 54.

distances as close as 1.3 Å, the protonated species remain bound with no rupture of the C−S bond and no dissociation of the adduct. We also generated profiles for acid attack of the flavin N^5 atom. However, all of our attempts for both the reduced and radical adducts resulted in the formation of the stable O^4-protonated species, which appears to shield N^5 from any approaching proton.

Base Attack. The most favorable reaction with OH^- for the reduced form leads to the rupture of the C−S bond with formation of the flavin N^5−CH_2OH species and liberation of the CH_3−S^- anion (−70 kJ/mol) (Figure S6). The reaction resulting in the rupture of the N^5−CH_2 bond upon hydroxide attack is also favorable, although it is much less exothermic (−14 kJ/mol). For the radical form, both reactions are favorable, but the second one is now much more exothermic (−128 vs −66 kJ/mol). Thus, the reduced form favors rupture of the C−S bond, whereas the radical form favors that of the N^5−CH_2 bond. As for acid attack, we generated energy profiles to obtain an estimate of the energy barriers to hydroxide attack on the C atom of the adduct. Depending on the initial orientation of the OH^- group, these profiles resulted in either the rupture of the adduct's N^5−C or of its C−S bonds in both the reduced and radical forms. In all cases, high barriers were obtained (between 90 and 150 kJ/mol).

CONCLUSIONS

TrmFO is a remarkable and unique enzyme. It uses a combination of a reduced FAD and the thiol group of a cysteine (Cys53) to stabilize a methylene group derived from CH_2THF.[9] Thus, the TrmFO−CH_2−FADH adduct, with the methylene bridging N^5 of the isoalloxazine ring and S from cysteine53, contains all of the ingredients to methylate the tRNA substrate. However, it is so stable in the absence of tRNA that it is present in significant amounts in freshly purified preparations of the enzyme, thus allowing the characterization of its structure and its chemical reactivity.[7,9] We proposed that it is the precursor of the methylating agent that is responsible for methylation of uridine at position 54 in tRNAs, thus forming the widely conserved m^5U_{54}. The same preparations also contain a stable and peculiar FAD-derived radical, the structure of which we have addressed here by spectroscopic analyses and DFT calculations. The last species is not competent for tRNA methylation.

Our experimental and theoretical data provide insights into how the methylene of the adduct is activated (Figure 4). We clearly show here that a protonation step is involved. Indeed, in the absence of tRNA, decomposition of the TrmFO−CH_2−FADH adduct into FAD, which is no longer covalently bound to the protein as shown by protein-denaturation experiments, occurs only at low pH under aerobic conditions, with the reaction rate increasing with decreased pH. We thus propose that upon protonation of the S_γ atom of Cys53, heterolytic

dx.doi.org/10.1021/bi4013879 | *Biochemistry* 2013, 52, 8949−8956

cleavage of the C−S bond is favored, generating the highly reactive $[FADH(N^5)=CH_2]^+$ iminium intermediate, which subsequently reacts with water and oxygen to yield FAD, presumably with parallel formation of formaldehyde and hydrogen peroxide (Figure 4A). This agrees with our previous work in which we showed that addition of formaldehyde into solutions of freshly purified enzyme greatly stabilized the TrmFO−CH_2−FADH adduct.[7] DFT calculations on a simple model of the methylating species in TrmFO are consistent with this proposal because they show that upon acid attack the reduced form of the model system undergoes a barrierless exothermic reaction in which the $[FADH(N^5)=CH_2]^+$ iminium is formed with liberation of the bound Cys residue (Figure S6). In contrast, calculations indicate that the N−CH_2−S moiety can be broken upon hydroxide attack in an exothermic reaction, but the barriers are high, correlating with the observation that the reaction is very slow at high pH (Figure S6).

In Figure 4B we propose that in the presence of the tRNA substrate the tRNA triggers the cysteine protonation step and that the iminium intermediate is the active methylating agent. This electrophilic species is then attacked by the negatively charged C5 of the uridine 54 substrate, previously activated by the addition of Cys226 at C6. Deprotonation at C5 of uridine within the hybrid intermediate TrmFO−tRNA−CH_2−FADH adduct leads to the heterolytic cleavage of the N_5−C bond. The resulting reduced $FADH_2$ finally reduces the exocyclic methylene on the nucleic base to generate m^5U_{54} after release of Cys226. Interestingly, the consumption of the TrmFO−CH_2−FADH adduct in the presence of tRNA proceeds with an observed rate constant ~40 times faster than that for its conversion into FAD in the absence of tRNA. This suggests that activation of the adduct in this case might be promoted by a nearby general acid catalyst like an active amino acid or even a nucleotide of the tRNA itself. This requires further investigation.

The stable organic radical species present in TrmFO, although catalytically incompetent, is also an intriguing compound. New analyses of the EPR and ENDOR associated spectra coupled with DFT calculations lead us now to assign unambiguously these spectra to a TrmFO−CH2−$FAD^\bullet$ radical that is simply derived from the TrmFO−CH_2−FADH adduct by a one-electron oxidation. A similar structure has been proposed for a radical in a LOV protein mutant.[28] This radical is highly stabilized and much less susceptible to protonation than the reduced adduct in the absence of tRNA. This is also consistent with DFT calculations that showed that the radical model undergoes a mildly exothermic protonation on the Cys Sγ atom but dissociation does not occur because this is an endothermic process. The very slow decomposition observed at high pH can be explained by an attack of the methylene group by a H_2O/OH^- molecule, leading to the neutral and oxygen-sensitive $FADH^\bullet$ radical and a labile Cys_{53}−S−CH_2OH that decomposes immediately into formaldehyde and Cys_{53}−SH. Again, this is in agreement with DFT calculations that suggest that the radical is more unstable in the presence of a hydroxide, although with high barriers to decomposition.

The proton-dependent activation of the TrmFO−CH_2−FADH adduct reported here presents striking analogies with that of methylenetetrahydrofolate used for example by methylenetetrahydrofolate reductase and thymidylate synthase:[29−33] (i) both species are stable and thus provide a mechanism for the enzyme to store safely an otherwise reactive methylene moiety; (ii) both species are further stabilized by addition of formaldehyde; (iii) in both cases, these storage forms are proposed to be converted into highly reactive $[N=CH_2]^+$ iminium intermediates that are the actual alkylating species; (iv) in both cases, these conversion reactions operate via protonation (protonation of N^{10} in CH_2THF and cleavage of the N^{10}−C bond or protonation of the S_γ atom of Cys53 and cleavage of the S−C bond in the TrmFO−CH_2−FADH adduct) (Figure 5). The newly discovered FAD-dependent

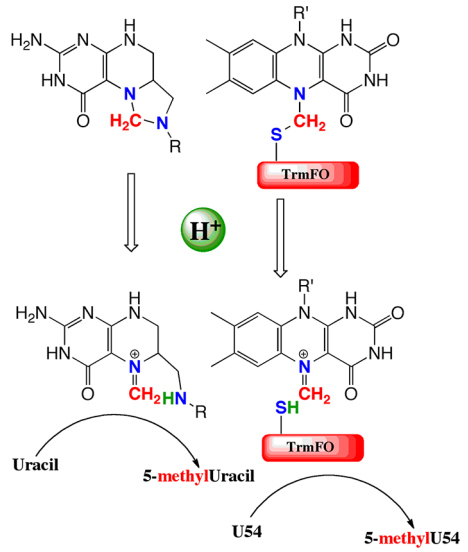

Figure 5. Mechanistic analogies in activation of methylating species in methylene-THF-dependent enzymes and in TrmFO.

methylating mechanism reported here thus establishes that not only folates but also flavins may be utilized by enzymes to store an active methylene group between two heteroatoms and activate it for methylation reactions. We fully expect that additional enzymes using this flavin-dependent mechanism will be discovered in the future.

■ ASSOCIATED CONTENT

Supporting Information

Radical model used for calculated B3LYP/6-31+ G(D,P), pH dependence of the optical spectra of TrmFO, denaturation of TrmFO by urea, kinetics of N5-alkylated FAD adduct conversion to oxidized FAD in the presence of urea, crystal structure of TrmFO, chemical structure of the flavin adducts used for the DFT calculations, and energetics diagrams of the methylating species as a function of the pH. This material is available free of charge via the Internet at http://pubs.acs.org.

■ AUTHOR INFORMATION

Corresponding Author

*E-mail: djemel.hamdane@college-de-france.fr; Phone: 33 1 44 27 12 54.

Funding

This work was supported by the French State Program 'Investissements d'Avenir' (Grant "LABEX DYNAMO", ANR-11-LABX-0011).

Notes

The authors declare no competing financial interest.

■ ACKNOWLEDGMENTS

We are grateful to Klaus Brettel (CEA Saclay, France) and André Eker (Erasmus University Medical Center, Rotterdam, The Netherlands) for providing samples of pure photolyase for the EPR/ENDOR studies.

■ REFERENCES

(1) Urbonavicius, J., Skouloubris, S., Myllykallio, H., and Grosjean, H. (2005) Identification of a novel gene encoding a flavin-dependent tRNA:m5U methyltransferase in bacteria—evolutionary implications. *Nucleic Acids Res. 33*, 3955−3964.

(2) Nishimasu, H., Ishitani, R., Yamashita, K., Iwashita, C., Hirata, A., Hori, H., and Nureki, O. (2009) Atomic structure of a folate/FAD-dependent tRNA T54 methyltransferase. *Proc. Natl. Acad. Sci. U.S.A. 106*, 8180−8185.

(3) Bjork, G. R. (1995) Genetic dissection of synthesis and function of modified nucleosides in bacterial transfer RNA. *Prog. Nucleic Acid Res. Mol. Biol. 50*, 263−338.

(4) Delk, A. S., Nagle, D. P., Jr., Rabinowitz, J. C., and Straub, K. M. (1979) The methylenetetrahydrofolate-mediated biosynthesis of ribothymidine in the transfer-RNA of *Streptococcus faecalis*: Incorporation of hydrogen from solvent into the methyl moiety. *Biochem. Biophys. Res. Commun. 86*, 244−251.

(5) Delk, A. S., Nagle, D. P., Jr., and Rabinowitz, J. C. (1980) Methylenetetrahydrofolate-dependent biosynthesis of ribothymidine in transfer RNA of *Streptococcus faecalis*. Evidence for reduction of the 1-carbon unit by FADH2. *J. Biol. Chem. 255*, 4387−4390.

(6) Yamagami, R., Yamashita, K., Nishimasu, H., Tomikawa, C., Ochi, A., Iwashita, C., Hirata, A., Ishitani, R., Nureki, O., and Hori, H. (2012) The tRNA recognition mechanism of folate/FAD-dependent tRNA methyltransferase (TrmFO). *J. Biol. Chem. 287*, 42480−42494.

(7) Hamdane, D., Guerineau, V., Un, S., and Golinelli-Pimpaneau, B. (2011) A catalytic intermediate and several flavin redox states stabilized by folate-dependent tRNA methyltransferase from *Bacillus subtilis*. *Biochemistry 50*, 5208−5219.

(8) Hamdane, D., Argentini, M., Cornu, D., Myllykallio, H., Skouloubris, S., Hui-Bon-Hoa, G., and Golinelli-Pimpaneau, B. (2011) Insights into folate/FAD-dependent tRNA methyltransferase mechanism: Role of two highly conserved cysteines in catalysis. *J. Biol. Chem. 286*, 36268−36280.

(9) Hamdane, D., Argentini, M., Cornu, D., Golinelli-Pimpaneau, B., and Fontecave, M. (2012) FAD/folate-dependent tRNA methyltransferase: Flavin as a new methyl-transfer agent. *J. Am. Chem. Soc. 134*, 19739−19745.

(10) Kealey, J. T., and Santi, D. V. (1991) Identification of the catalytic nucleophile of tRNA (m5U54)methyltransferase. *Biochemistry 30*, 9724−9728.

(11) Liu, Y., and Santi, D. V. (2000) m5C RNA and m5C DNA methyl transferases use different cysteine residues as catalysts. *Proc. Natl. Acad. Sci. U.S.A. 97*, 8263−8265.

(12) King, M. Y., and Redman, K. L. (2002) RNA methyltransferases utilize two cysteine residues in the formation of 5-methylcytosine. *Biochemistry 41*, 11218−11225.

(13) Alian, A., Lee, T. T., Griner, S. L., Stroud, R. M., and Finer-Moore, J. (2008) Structure of a TrmA-RNA complex: A consensus RNA fold contributes to substrate selectivity and catalysis in m5U methyltransferases. *Proc. Natl. Acad. Sci. U.S.A. 105*, 6876−6881.

(14) Hamdane, D., Skouloubris, S., Myllykallio, H., and Golinelli-Pimpaneau, B. (2010) Expression and purification of untagged and histidine-tagged folate-dependent tRNA:m5U54 methyltransferase from *Bacillus subtilis*. *Protein Expression Purif. 73*, 83−89.

(15) Un, S., Dorlet, P., and Rutherford, A. W. (2001) A high-field EPR tour of radicals in photosystems I and II. *Appl. Magn. Reson. 21*, 341−361.

(16) Un, S. (2005) The g-values and hyperfine coupling of amino acid radicals in proteins: comparison of experimental measurements with ab initio calculations. *Magn. Reson. Chem. 43*, S229−S239.

(17) Weigend, F., and Ahlrichs, R. (2005) Balanced basis sets of split valence, triple zeta valence and quadruple zeta valence quality for H to Rn: Design and assessment of accuracy. *Phys. Chem. Chem. Phys. 7*, 3297−3305.

(18) Sinnecker, S., Rajendran, A., Klamt, A., Diedenhofen, M., and Neese, F. (2006) Calculation of solvent shifts on electronic g-tensors with the conductor-like screening model (COSMO) and its self-consistent generalization to real solvents (direct COSMO-RS). *J. Phys. Chem. A 110*, 2235−2245.

(19) Becke, A. D. (1988) Density-functional exchange-energy approximation with correct asymptotic behavior. *Phys. Rev. A 38*, 3098−3100.

(20) Lee, C., Yang, W., and Parr, R. G. (1988) Development of the Colle-Salvetti correlation-energy formula into a functional of the electron density. *Phys. Rev. B: Condens Matter Mater. Phys. 37*, 785−789.

(21) Neese, F. (2011) The Orca Program System. *Wiley Interdiscip. Rev.: Comput. Mol. Sci. 2*, 73−78.

(22) Okafuji, A., Schnegg, A., Schleicher, E., Mobius, K., and Weber, S. (2008) G-tensors of the flavin adenine dinucleotide radicals in glucose oxidase: A comparative multifrequency electron paramagnetic resonance and electron-nuclear double resonance study. *J. Phys. Chem. B 112*, 3568−3574.

(23) Barquera, B., Morgan, J. E., Lukoyanov, D., Scholes, C. P., Gennis, R. B., and Nilges, M. J. (2003) X- and W-band EPR and Q-band ENDOR studies of the flavin radical in the Na^+-translocating NADH:quinone oxidoreductase from *Vibrio cholerae*. *J. Am. Chem. Soc. 125*, 265−275.

(24) Schleicher, E., Wenzel, R., Ahmad, M., Batschauer, A., Essen, L. O., Hitomi, K., Getzoff, E. D., Bittl, R., Weber, S., and Okafuji, A. (2010) The electronic state of flavoproteins: Investigations with proton electron−nuclear double resonance. *Appl. Magn. Reson. 37*, 339−352.

(25) Kay, C. W., Bittl, R., Bacher, A., Richter, G., and Weber, S. (2005) Unambiguous determination of the g-matrix orientation in a neutral flavin radical by pulsed electron-nuclear double resonance at 94 GHz. *J. Am. Chem. Soc. 127*, 10780−10781.

(26) Schleicher, E., Hitomi, K., Kay, C. W., Getzoff, E. D., Todo, T., and Weber, S. (2007) Electron nuclear double resonance differentiates complementary roles for active site histidines in (6-4) photolyase. *J. Biol. Chem. 282*, 4738−4747.

(27) Heller, C., and McConnel, H. M. (1960) Radiation damage in organic crystals. II. Electron spin resonance of $(CO_2H)CH_2CH(CO_2H)$ in β-succinic acid. *J. Phys. Chem. 32*, 1535−1539.

(28) Bittl, R., Kay, C. W., Weber, S., and Hegemann, P. (2003) Characterization of a flavin radical product in a C57M mutant of a LOV1 domain by electron paramagnetic resonance. *Biochemistry 42*, 8506−8512.

(29) Matthews, D. A., Appelt, K., Oatley, S. J., and Xuong, N. H. (1990) Crystal structure of *Escherichia coli* thymidylate synthase containing bound 5-fluoro-2′-deoxyuridylate and 10-propargyl-5,8-dideazafolate. *J. Mol. Biol. 214*, 923−936.

(30) Perry, K. M., Carreras, C. W., Chang, L. C., Santi, D. V., and Stroud, R. M. (1993) Structures of thymidylate synthase with a C-terminal deletion: Role of the C-terminus in alignment of 2′-deoxyuridine 5′-monophosphate and 5,10-methylenetetrahydrofolate. *Biochemistry 32*, 7116−7125.

(31) Zapf, J. W., Weir, M. S., Emerick, V., Villafranca, J. E., and Dunlap, R. B. (1993) Substitution of glutamine for glutamic acid-58 in *Escherichia coli* thymidylate synthase results in pronounced decreases in catalytic activity and ligand binding. *Biochemistry 32*, 9274−9281.

(32) Carreras, C. W., and Santi, D. V. (1995) The catalytic mechanism and structure of thymidylate synthase. *Annu. Rev. Biochem. 64*, 721−762.

(33) Hyatt, D. C., Maley, F., and Montfort, W. R. (1997) Use of strain in a stereospecific catalytic mechanism: Crystal structures of *Escherichia coli* thymidylate synthase bound to FdUMP and methylenetetrahydrofolate. *Biochemistry 36*, 4585−4594.